Copy 312
RM L55J06

NACA

RESEARCH MEMORANDUM

LOW-SPEED STATIC STABILITY CHARACTERISTICS OF A COMPLETE MODEL WITH AN M-WING IN MID AND HIGH POSITIONS AND WITH THREE HORIZONTAL-TAIL HEIGHTS

By Paul G. Fournier

Langley Aeronautical Laboratory
Langley Field, Va.

NATIONAL ADVISORY COMMITTEE
FOR AERONAUTICS

WASHINGTON
January 24, 1956

NATIONAL ADVISORY COMMITTEE FOR AERONAUTICS

RESEARCH MEMORANDUM

LOW-SPEED STATIC STABILITY CHARACTERISTICS OF A COMPLETE MODEL WITH AN M-WING IN MID AND HIGH POSITIONS AND WITH THREE HORIZONTAL-TAIL HEIGHTS

By Paul G. Fournier

SUMMARY

An investigation was made of the low-speed static longitudinal and lateral stability characteristics of a model having an M-wing in mid and high positions and with three horizontal-tail heights. The wing, having its sweep discontinuity located at 40-percent wing semispan, had an aspect ratio of 6, a taper ratio of 0.60, NACA 65A009 airfoil sections parallel to the plane of symmetry, and $\pm 45^{\circ}$ sweep of the quarter-chord lines.

The high wing improved the longitudinal stability characteristics of the mid-tail configuration and, in effect, made the stability characteristics of the mid-tail configuration approach the more favorable pitching-moment characteristics of the low-tail configuration. For either the mid- or high-wing arrangements, it appears that some longitudinal instability near maximum lift may exist when the T-tail configuration is used.

The results indicate that raising the wing from the mid to the high position provided a slight decrease in drag at the higher lift coefficients, but essentially caused no change in maximum lift-drag ratios. The results also indicate that, although raising the wing from the mid to the high position reduced the directional stability of the tail-on configurations by a substantial amount at low lift coefficients, the effects of wing height were negligible at high lift coefficients. All tail-on configurations were directionally stable throughout the lift-coefficient range, including the stall. Also, a positive increment of effective dihedral, over that for the midwing configuration, was noted for the wing-fuselage configuration with the high wing and was in the same order as would be expected for swept or unswept wings.

INTRODUCTION

Results of tests to determine the effect of spanwise location of the sweep discontinuity of M- and W-wings on the static longitudinal and lateral stability characteristics of a complete model are presented in references 1 and 2, respectively. The results show that these wings (especially the M type) provide favorable longitudinal stability characteristics and good directional stability at high lift. Little advantage in stability appeared to result from locating the sweep discontinuity of M-wings outboard of the 40-percent-semispan location; and since, from divergence-speed considerations for a given ratio of torsional stiffness to bending stiffness, it is desirable to keep the sweptforward panels of an M-wing relatively small (ref. 3), the M-wing with its sweep discontinuity at 40-percent semispan was selected for further study.

During the tests of reference 1, it was noted that the flow above the sweptforward panel was directed toward the fuselage at positive angles of attack and that separation at the wing root occurred at low angles of attack. It was reasoned that flow separation at the wing root might be delayed somewhat by mounting the wing with its upper surface tangent to the top of the fuselage, rather than having the chord plane of the wing located on the fuselage center line. The present investigation therefore was intended to determine any possible advantages of raising the wing height and, in addition, to extend the range of tail height covered in references 1 and 2 to include a horizontal tail mounted at the top of the vertical tail (T-tail).

The M-wing tested had an aspect ratio of 6, a taper ratio of 0.60, NACA 65A009 airfoil sections parallel to the plane of symmetry, and $\pm 45^\circ$ sweep of the quarter-chord line. The data presented herein were obtained from tests in the Langley 300 MPH 7- by 10-foot wind tunnel.

COEFFICIENTS AND SYMBOLS

The stability system of axes used for the presentation of the data and the positive direction of forces, moments, and angles are shown in figure 1. All moments of the basic data are referred to the quarter-chord point of the wing mean aerodynamic chord.

b wing span, ft

C_D drag coefficient, $C_D = -C_X$

C_L lift coefficient, $\frac{\text{Lift}}{qS}$

C_l rolling-moment coefficient, $\frac{\text{Rolling moment}}{qSb}$

C_m pitching-moment coefficient, $\frac{\text{Pitching moment}}{qS\bar{c}}$

C_n yawing-moment coefficient, $\frac{\text{Yawing moment}}{qSb}$

C_X longitudinal-force coefficient, $\frac{\text{Longitudinal force}}{qS}$

C_Y lateral-force coefficient, $\frac{\text{Lateral force}}{qS}$

C_{l_β} rolling moment due to sideslip, $\frac{\partial C_l}{\partial \beta}$ per degree

C_{n_β} yawing moment due to sideslip, $\frac{\partial C_n}{\partial \beta}$ per degree

C_{Y_β} lateral force due to sideslip, $\frac{\partial C_Y}{\partial \beta}$ per degree

$\bar{c}$ wing mean aerodynamic chord, ft

$\bar{c}_t$ horizontal tail mean aerodynamic chord, ft

i_t angle of incidence of the horizontal tail with respect to fuselage center line, degree

l_t tail length, distance from $\frac{\bar{c}}{4}$ to $\frac{\bar{c}_t}{4}$, ft

q free-stream dynamic pressure, $\frac{\rho V^2}{2}$, lb/sq ft

S wing area, sq ft

V free-stream velocity, ft/sec

α angle of attack, degree

β angle of sideslip, degree

Δ_w increment due to wing height

Δ_v increment due to the contribution of the vertical tail (WFV-WF)

ρ mass density of air, slugs/cu ft

Notation of configuration:

F	fuselage
H_L	horizontal tail, low tail
H_M	horizontal tail, mid tail
H_T	horizontal tail, T-tail
T.O.	horizontal tail off
V	original vertical tail
V_1	alternate vertical tail
W	wing

MODEL AND APPARATUS

The present investigation is a detailed study of a configuration having an M-wing with sweep discontinuity at 40-percent semispan, for which some results have been presented in references 1 and 2. The wing had an aspect ratio of 6, a taper ratio of 0.60, NACA 65A009 airfoil sections parallel to the plane of symmetry, and $\pm 45^\circ$ sweep of the quarter-chord lines. The horizontal tail had an aspect ratio of 4, a taper ratio of 0.60, 45° sweepback of the quarter-chord line, and NACA 65A006 airfoil sections parallel to the plane of symmetry. The fuselage had a fineness ratio of 10.86 which was achieved by cutting off a portion of the rear of a fineness-ratio-12 closed body of revolution, the ordinates of which are presented in reference 1. The fuselage was constructed of wood and the wing was constructed of wood-bonded-to-steel reinforcing spars. A three-view drawing of the model with the wing at mid height is shown in figure 2.

The longitudinal reference location of the quarter-chord point of the wing mean aerodynamic chord, about which all moments and forces were taken, remained the same for both wing heights. The original model was constructed so that tests could be made with the horizontal tail at two tail heights, a low tail located on the mid-wing chord plane extended and a high tail located 20.83-percent wing semispan above the mid-wing chord plane extended. (See refs. 1 and 2.)

In addition to the low tail and high tail, the present investigation includes tests of the model with a T-tail located 47-percent wing semispan above the mid-wing chord plane extended. This was achieved by using an alternate vertical tail which allowed the horizontal tail to be mounted as a T-tail. In order to clarify the notation of the location of the horizontal tail in the present paper, the original high tail (refs. 1 and 2) will be called the mid tail. The horizontal tail heights will now be designated as a low-tail H_L, a mid-tail H_M, and a T-tail H_T.

Details of the vertical location of the wing and the vertical locations of the horizontal tail, including the alternate vertical tail, are presented in figure 3.

The model was mounted on a single-strut support, which was in turn fastened to the mechanical balance system of the Langley 300 MPH 7- by 10-foot tunnel.

TESTS AND CORRECTIONS

All tests were made at a dynamic pressure of 45.22 pounds per square foot, which for average tests conditions corresponds to a Mach number of about 0.17 and a Reynolds number of 1.27×10^6 based on the wing mean aerodynamic chord of 1.02 feet.

The present investigation consists of tests made to determine both the lateral and longitudinal static stability characteristics of the model with three tail heights. The parameters C_{l_β}, C_{n_β}, and C_{Y_β} were determined from tests at sideslip angles of $\pm 5^\circ$ through the angle-of-attack range from approximately -4° to 32°. The angle of attack, longitudinal force (-drag), and horizontal-tail-on pitching moment have been corrected for jet-boundary effects on the basis of unswept-wing theory by the method of reference 4. Reference 5 shows that the effect of sweep on these corrections is small. The dynamic pressure and drag coefficient have been corrected for blocking caused by the model and its wake by the method of reference 6.

Vertical buoyancy on the support strut, tunnel airflow misalinement, and longitudinal pressure gradient have been accounted for in the computation of the data. These data have not been corrected for the tares caused by the model-support strut; however, tare tests of a similar complete-model configuration have indicated that the tares corresponding to the lateral coefficients are small, that the correction to longitudinal force coefficient is about 0.009 at zero lift, and that the correction to pitching-moment coefficient is small and independent of angle of attack through most of the range.

RESULTS AND DISCUSSION

The basic longitudinal stability results are presented in figures 4 and 5 and are summarized as a function of lift coefficient together with data from reference 1 in figure 6. The basic lateral stability characteristics are presented in figure 7 and are summarized as a function of lift coefficient together with data from reference 2 in figures 8 and 9.

Longitudinal Stability Characteristics

The pitching-moment characteristics included in the basic data (figs. 4 and 5) represent a center-of-gravity location at $0.25\bar{c}$. The static margin, therefore, varied somewhat with wing height and with tail configuration. In order to provide comparisons of pitching-moment curves under fairly realistic conditions, the summary data have been transferred to a center-of-gravity location such that a static margin of $0.10\bar{c}$ is obtained for all configurations having $i_t = 0^\circ$ at zero lift (fig. 6).

Complete-model configuration.- Comparison of the longitudinal stability data of the complete model with the M-wing (static margin $0.10\bar{c}$), presented in parts (a) and (b) of figure 6, shows that the variation of wing height within the range considered had little effect on the overall pitching-moment characteristics for either the low-tail or T-tail configuration, except that the high wing with the T-tail showed some improvement above 28° angle of attack. However, the high wing improved the longitudinal stability characteristics of the mid-tail configuration and in effect made the stability characteristics of the mid-tail configuration approach the more favorable pitching-moment characteristics of the low-tail configuration. This effect is similar to that noted in previous investigations for several different configurations. (For instance, see ref. 7.)

The effect of wing height on the lift-curve slope of the model with the various horizontal-tail heights (fig. 6(c)) is small. The drag polars (fig. 6(d)) indicate that the maximum lift-drag ratio is about the same for both wing heights but the high wing showed a slight decrease in longitudinal force at the higher lift coefficients for all the horizontal-tail heights.

Results of some tests (not presented) with tufts attached to the upper surface of the wing indicated that flow separation at the wing root was delayed somewhat by moving the wing to the high position. This probably results from the reduced restriction to the flow above the wing surface at the plane of symmetry due to the absence of any part of the fuselage.

Although the vertical tail for the T-tail configuration was not the same as for the low- and mid-tail configurations (fig. 3), it is felt that this difference would have a negligible effect on the longitudinal data presented herein.

Lateral Stability Characteristics

The basic data of the aerodynamic characteristics in sideslip of the model with the high wing as well as data with three horizontal-tail heights (low tail, mid tail, and T-tail) are presented in figure 7. It should be pointed out that there can be no direct comparison of the lateral stability characteristics between the T-tail and the low-tail and mid-tail configurations because of the difference in the vertical tail used with the T-tail configuration. Therefore, the discussion of the lateral stability characteristics will not include a discussion of the contribution of the alternate vertical tail $\left(\Delta_{v_1}\right)$ to the lateral stability parameters.

Comparison of results for the mid- and high-wing configurations are presented in figure 8. The largest effect of wing height on the aerodynamic characteristics in sideslip of the WF configuration (fig. 8(a)) is in the change of the effective dihedral C_{l_β}. At zero angle of attack, the high wing contributes a positive increment of effective dihedral, $-C_{l_\beta}$. This effect is as would be expected for swept or unswept wings (see ref. 8) and results from the cross flow about the yawed fuselage which induces a positive angle of attack for the leading wing (increased lift) and a negative angle of attack for the trailing wing (loss in lift) for the high-wing configuration. The opposite would be true if a low-wing configuration had been investigated. The experimental value of $\Delta_w C_{l_\beta}$ for the wing-fuselage configuration with the high wing is equal to -0.00066 and is in reasonably good agreement with the theoretical value $\Delta_w C_{l_\beta} = -0.00075$ from reference 8.

In general, the addition of the horizontal tails, especially the mid tail, reduced the effect of wing height on C_{l_β}. The increment in C_{l_β} due to the addition of the mid tail for the high-wing configuration is positive, whereas for the mid wing it is negative, thereby almost completely compensating the $\Delta_w C_{l_\beta}$ of the WFV configuration. The increments in C_{l_β} due to the addition of the T-tail for both wing heights are negative but of different magnitude such that $\Delta_w C_{l_\beta}$ for

the $WFVH_T$ configuration is considerably smaller than for the WFV configuration. However, the increment in C_{l_β} due to the low tail for both wing heights was approximately the same so that $\Delta_w C_{l_\beta}$ for the $WFVH_L$ configuration is only slightly less than $\Delta_w C_{l_\beta}$ for the WFV configuration. These effects may be due to the wing-body interference of the high wing which produces a vortex in a direction such that if a horizontal tail were located above this vortex, for example the mid tail and T-tail, a rolling moment would result that would have a tendency to compensate the effect of wing height on C_{l_β}.

It was noted that raising the wing from the mid to the high position reduced the directional stability of the tail-on configurations by a substantial amount at low lift coefficients, whereas the effects of wing height were negligible at high lift coefficients. All tail-on configurations were directionally stable throughout the lift-coefficient range, including the stall.

Figure 9 presents the vertical-tail contribution (WFV-WF) to the lateral parameters C_{l_β}, C_{n_β}, and C_{Y_β} for the WFV configuration. This figure shows that when the wing is moved from the mid to the high position the vertical-tail contribution to C_{Y_β} and C_{n_β} is adversely affected while C_{l_β} is changed only an insignificant amount. The decrements in C_{Y_β} and C_{n_β} are due to the increased sidewash from the wing in the high position decreasing the effective angle of attack of the vertical tail. Therefore it would seem that from the $\Delta_v C_{l_\beta}$ curve the high wing sidewash has its greatest effect on the lower sections of the vertical tail since the rolling moment due to the vertical tail remains essentially the same for either wing height.

CONCLUSIONS

Results of a low-speed wind-tunnel investigation of a complete-model configuration having an M-wing mounted in mid and high positions and three horizontal-tail heights indicate the following conclusions:

1. The high wing improved the longitudinal stability characteristics of the mid-tail configuration and, in effect, made the stability characteristics of the mid-tail configuration approach the more favorable pitching-moment characteristics of the low-tail configuration. For either the mid- or high-wing arrangements, it appears that some longitudinal

instability near maximum lift existed when the T-tail configuration was used.

2. Raising the wing from the mid to the high position provided a slight decrease in drag at the higher lift coefficients, but caused essentially no change in maximum lift-drag ratio.

3. Although raising the wing from the mid to the high position reduced the directional stability of the tail-on configurations by a substantial amount at low lift coefficients, the effects of wing height were negligible at high lift coefficients. All tail-on configurations were directionally stable throughout the lift-coefficient range, including the stall.

4. A positive increment of effective dihedral over that for the mid-wing configuration was noted for the wing-fuselage configuration with the high wing and was in the same order as would be expected for swept or unswept wings.

Langley Aeronautical Laboratory,
National Advisory Committee for Aeronautics,
Langley Field, Va., October 18, 1955.

REFERENCES

1. Fournier, Paul G.: Effects of Spanwise Location of Sweep Discontinuity on the Low-Speed Longitudinal Stability Characteristics of a Complete Model With Wings of M and W Plan Form. NACA RM L54K23, 1955.

2. Fournier, Paul G.: Effects of Spanwise Location of Sweep Discontinuity on the Low-Speed Static Lateral Stability Characteristics of a Complete Model With Wings of M and W Plan Form. NACA RM L55D22, 1955.

3. Diederich, Franklin W., and Foss, Kenneth A.: Static Aeroelastic Phenomena of M-, W-, and Λ-Wings. NACA RM L52J21, 1953.

4. Gillis, Clarence L., Polhamus, Edward C., and Gray, Joseph L., Jr.: Charts for Determining Jet-Boundary Corrections for Complete Models in 7- by 10-Foot Closed Rectangular Wind Tunnels. NACA WR L-123, 1945. (Formerly NACA ARR L5G31.)

5. Polhamus, Edward C.: Jet-Boundary-Induced-Upwash Velocities for Swept Reflection-Plane Models Mounted Vertically in 7- by 10-Foot, Closed, Rectangular Wind Tunnels. NACA TN 1752, 1948.

6. Herriot, John G.: Blockage Corrections for Three-Dimensional-Flow Closed-Throat Wind Tunnels, With Consideration of the Effect of Compressibility. NACA Rep. 995, 1950. (Supersedes NACA RM A7B28.)

7. Neely, Robert H., and Griner, Roland F.: Summary and Analysis of Horizontal-Tail Contribution to Longitudinal Stability of Swept-Wing Airplanes at Low Speeds. NACA RM L55E23a, 1955.

8. Jacobs, W.: Lift and Moment Changes Due to the Fuselage for a Yawed Aeroplane With Unswept and Swept Wings. Rep. No. 34, Aero. Res. Inst. of Sweden (Stockholm), 1950.

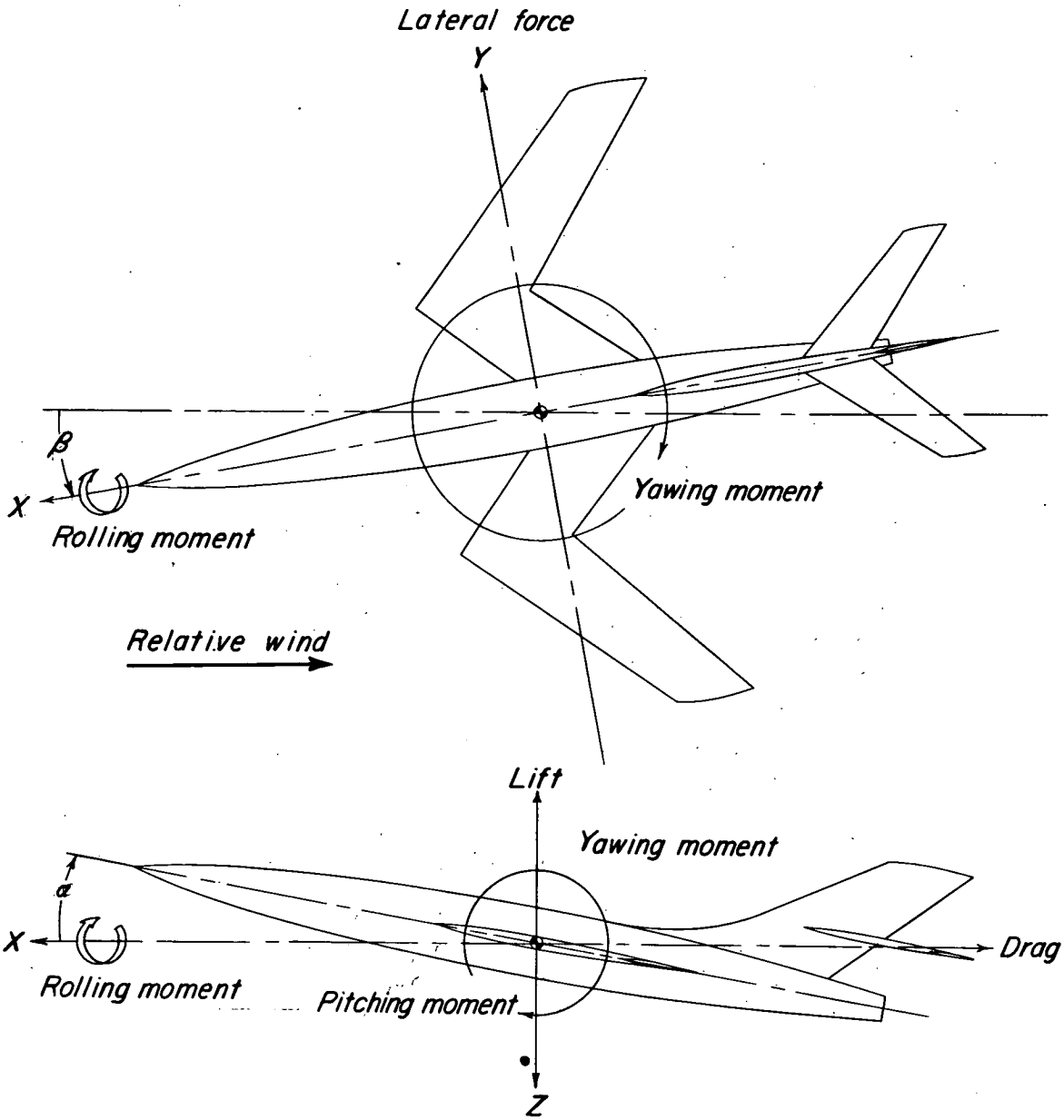

Figure 1.- Stability system of axes showing positive direction of forces, moments, and angles.

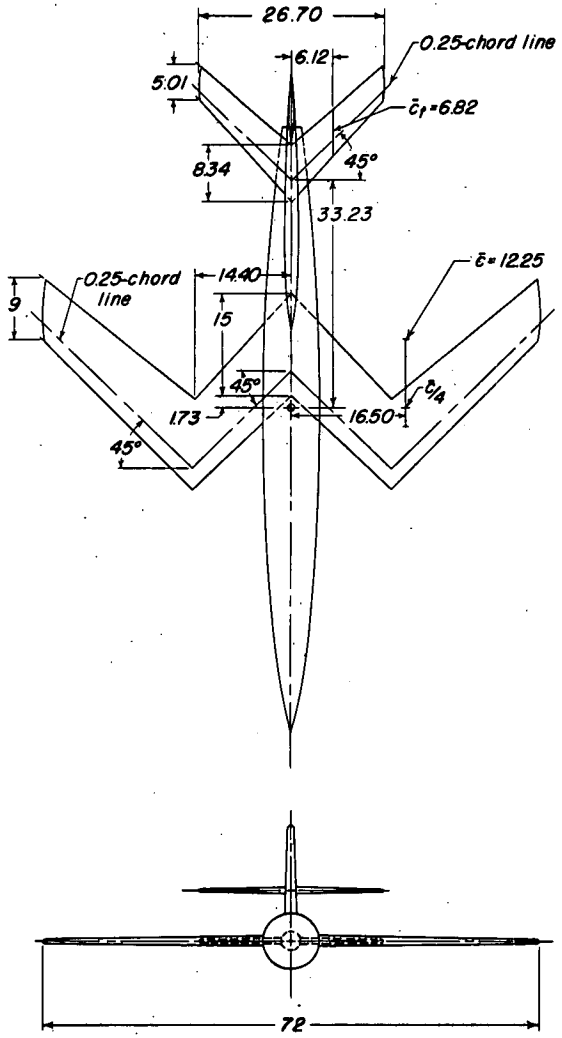

Physical Characteristics

Wing:	
Sweep of $c/4$ inboard panel, deg	-45
Sweep of $c/4$ outboard panel, deg	45
Area, sq ft	6
Span, ft	6
Aspect ratio	6
Taper ratio	0.60
Mean aerodynamic chord, ft	1.02
Incidence, deg	0
Dihedral, deg	0
Airfoil section parallel to plane of symmetry	65A009
Horizontal tail:	
Area, sq ft	1.24
Aspect ratio	4.00
Airfoil section parallel to plane of symmetry	NACA 65A006
Vertical tail:	
Area, sq ft	1.69
Aspect ratio	1.18
Airfoil section parallel to plane of symmetry	63A009

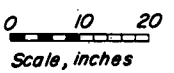

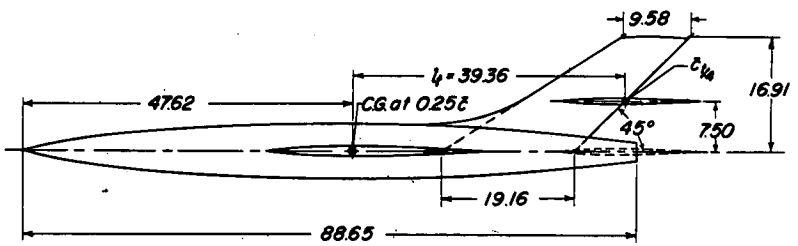

Figure 2.- General arrangement of test model with M-wing.

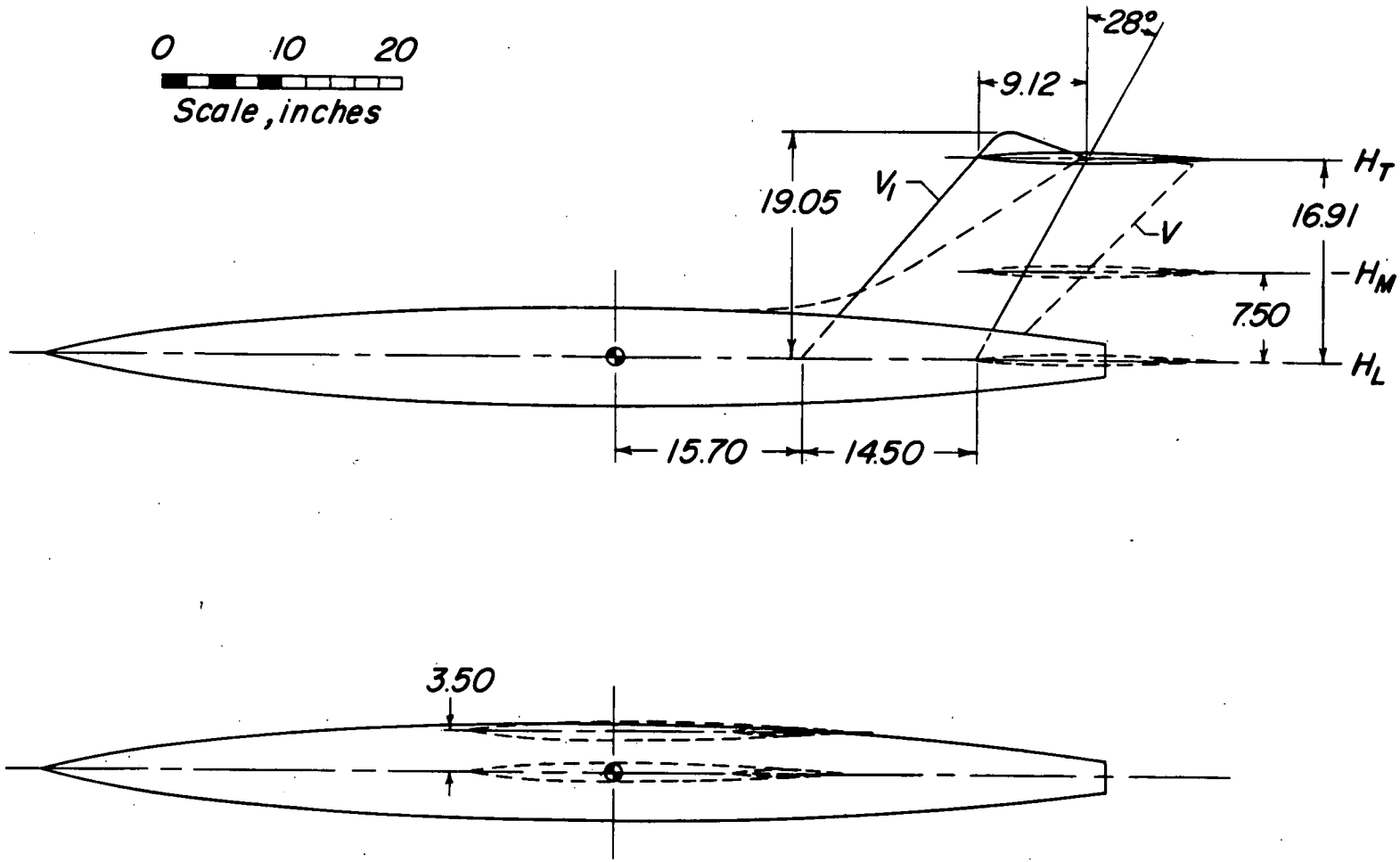

Figure 3.- Detail of tail height and wing height.

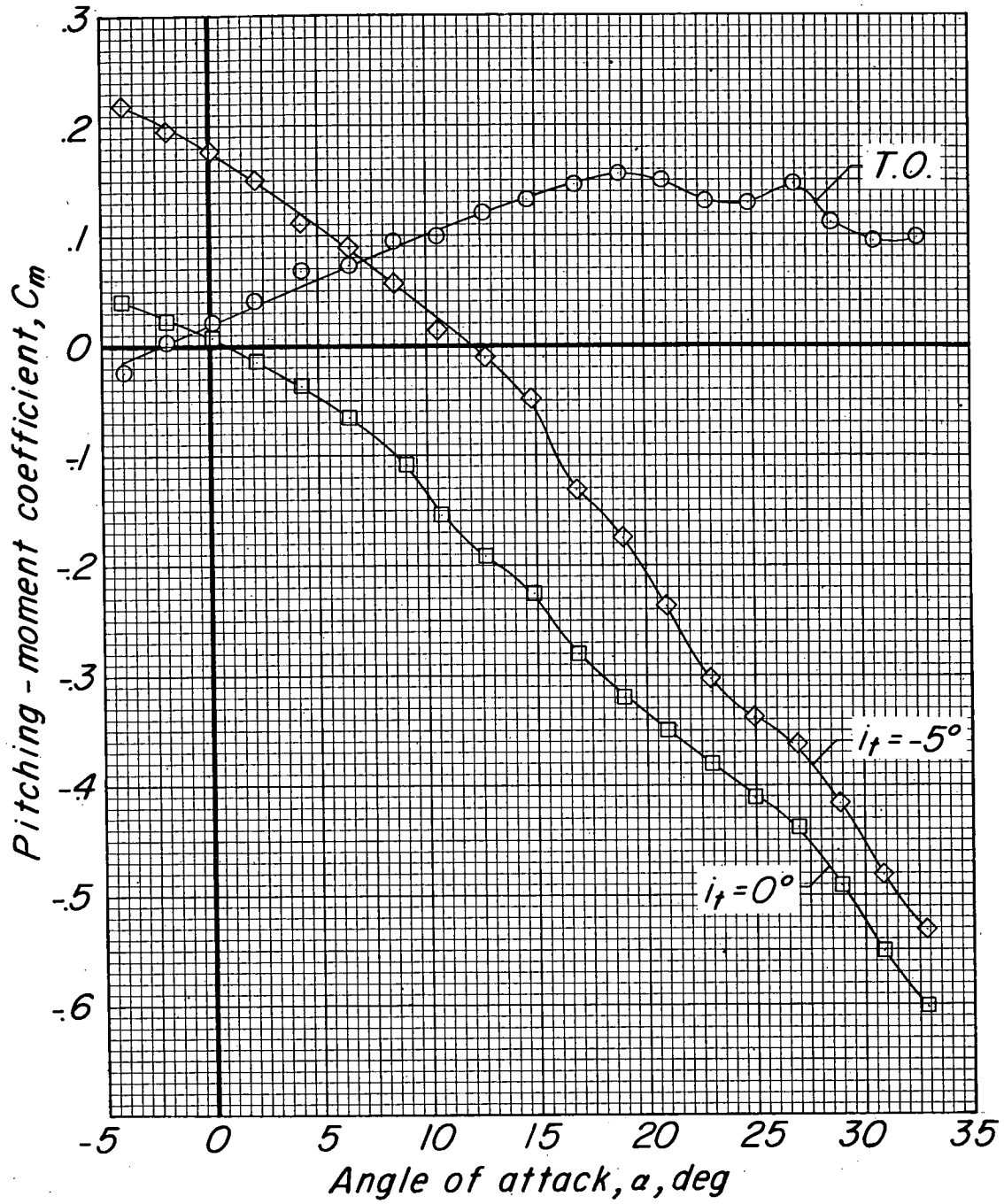

(a) Low tail.

Figure 4.- Effect of horizontal-tail incidence on aerodynamic characteristics of model with high M-wing.

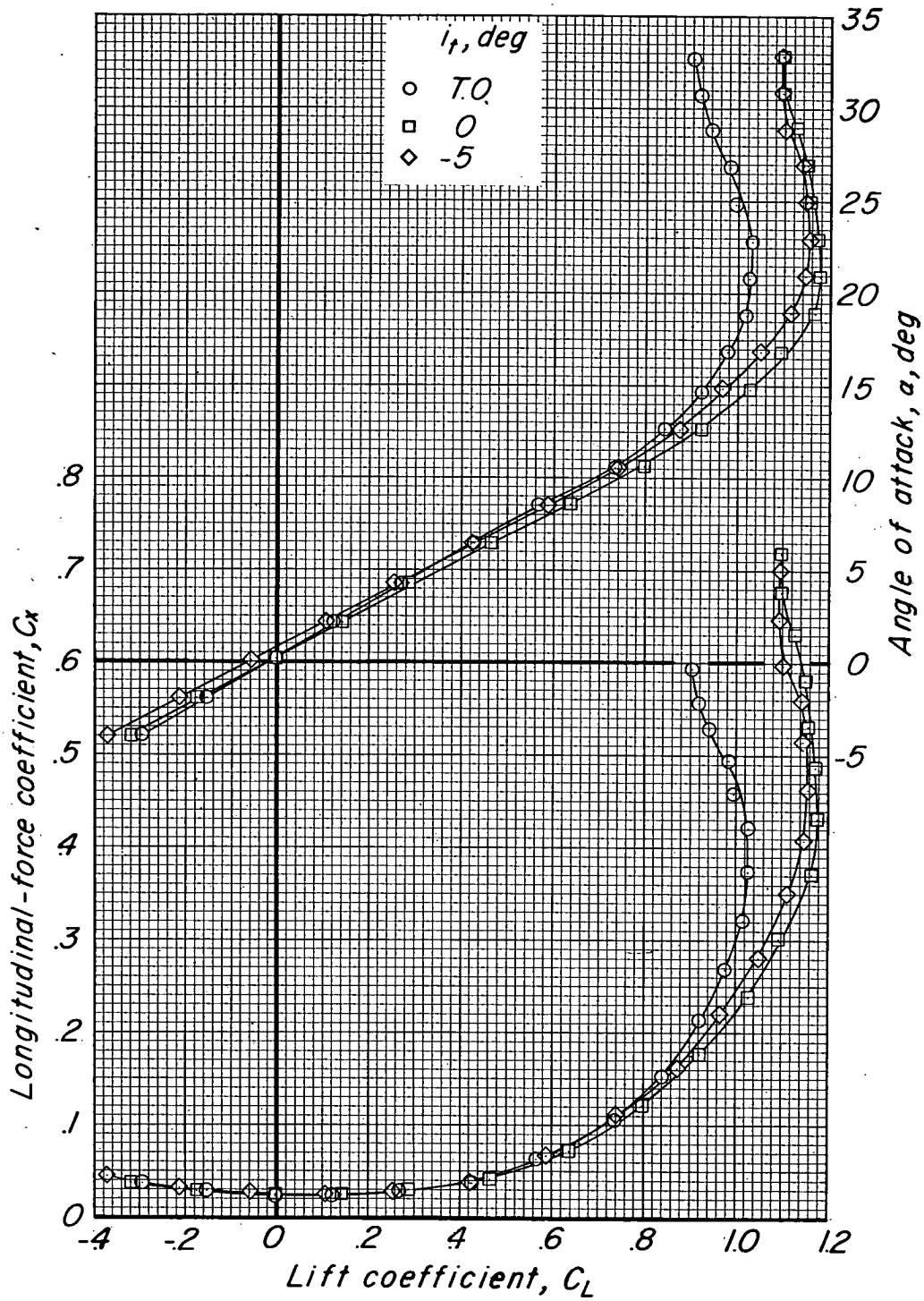

(a) Low tail. Concluded.

Figure 4.- Continued.

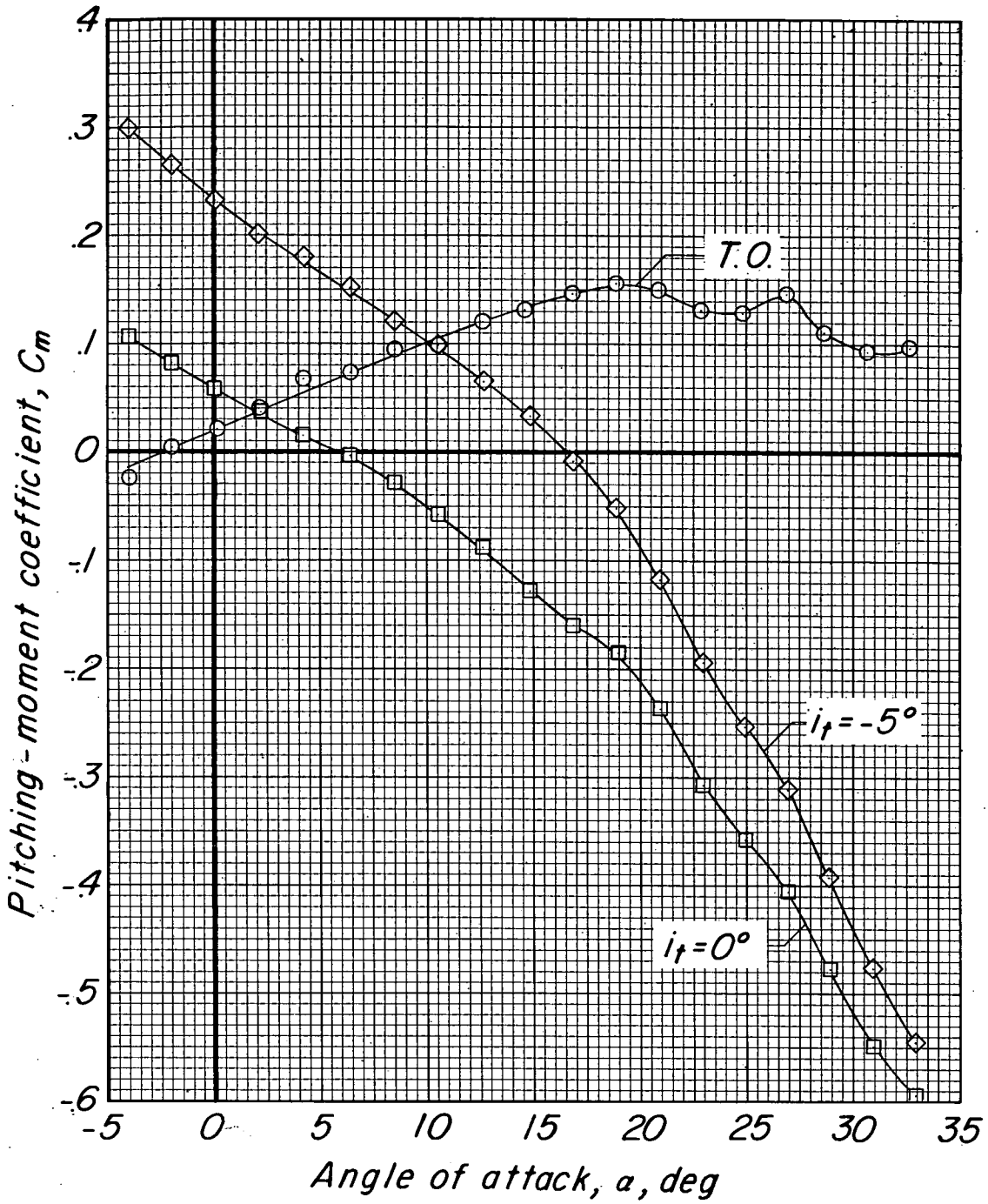

(b) Mid tail.

Figure 4.- Continued.

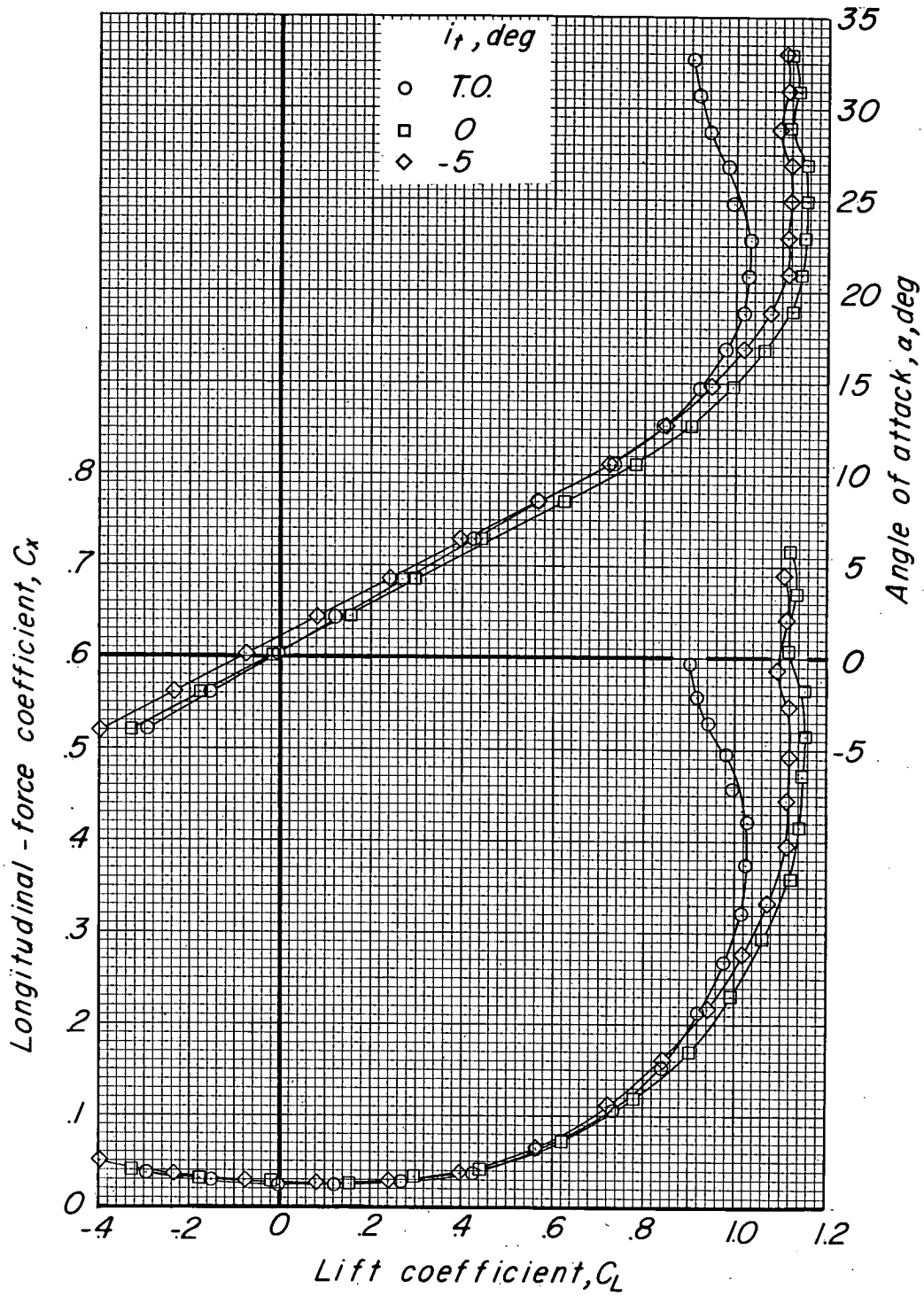

(b) Mid tail. Concluded.

Figure 4.- Continued.

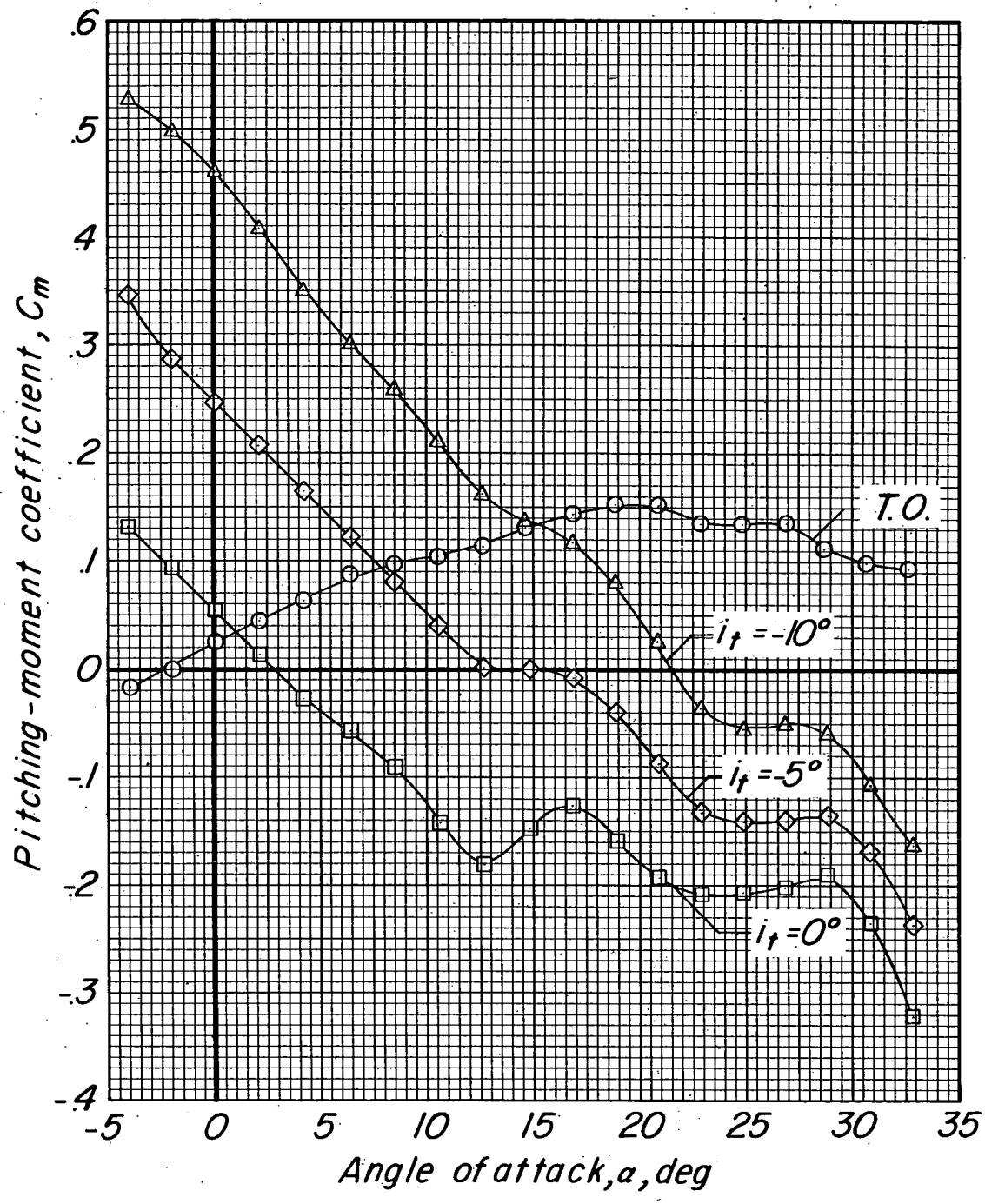

(c) T-tail.

Figure 4.- Continued.

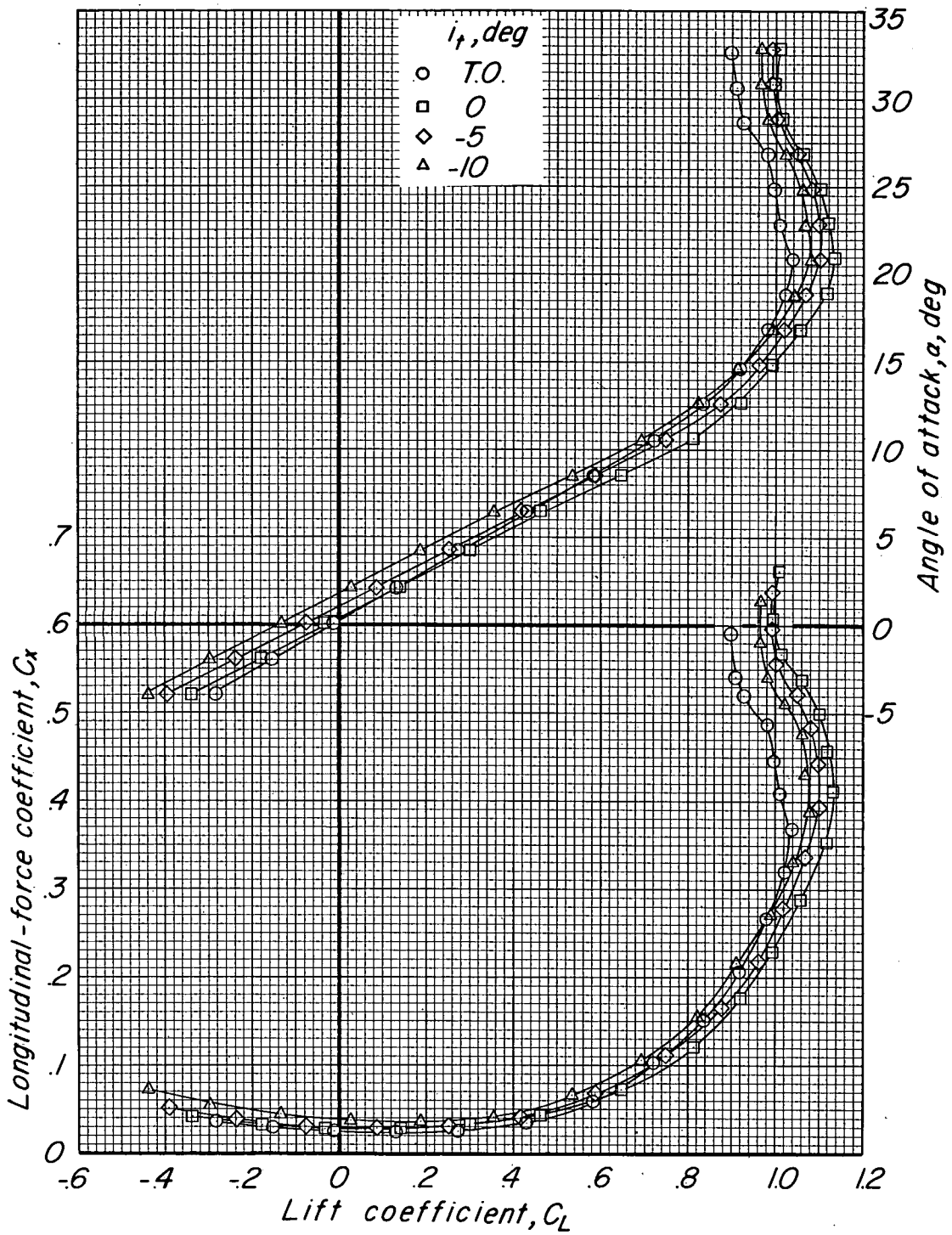

(c) T-tail. Concluded.

Figure 4.- Concluded.

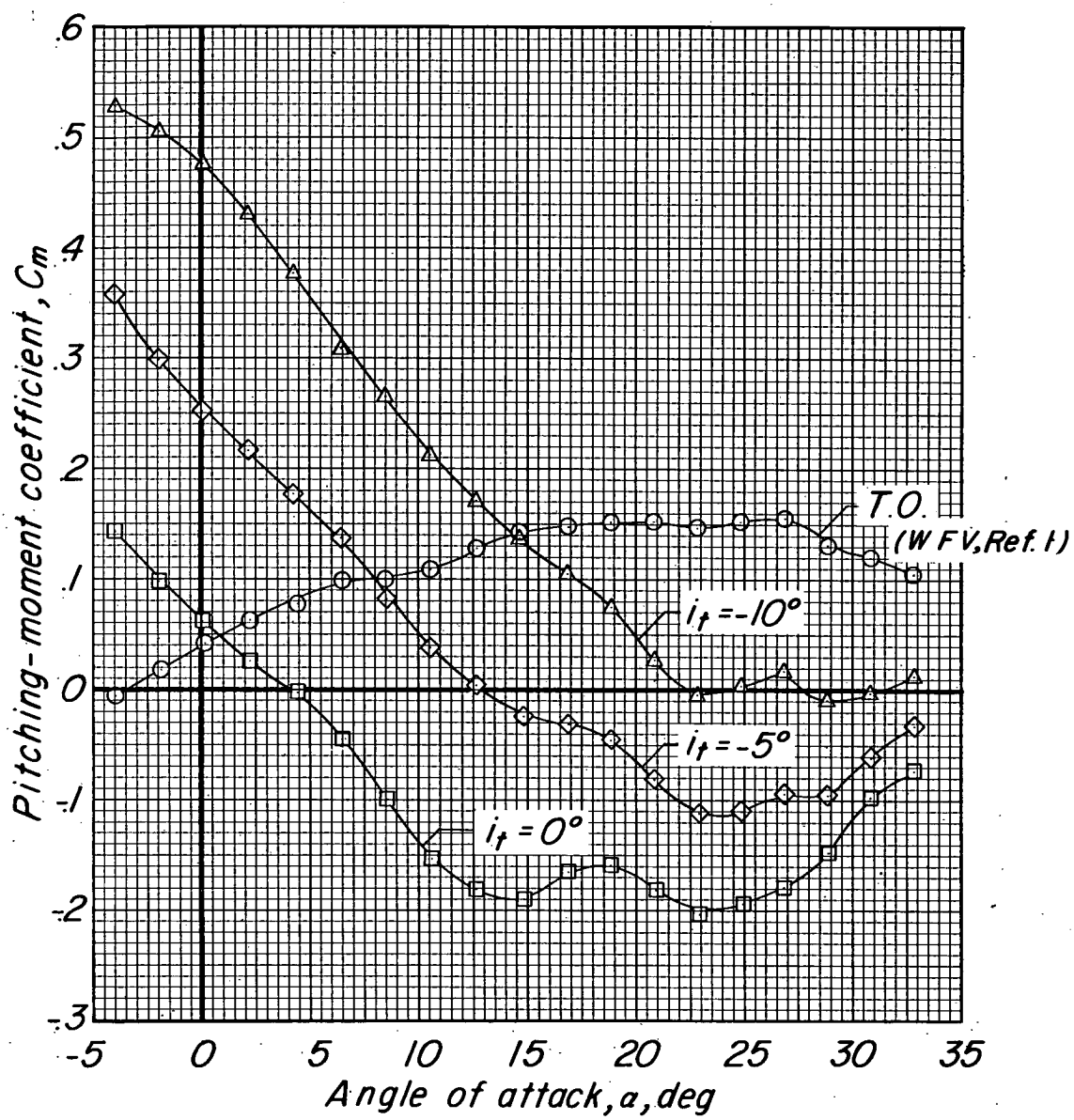

Figure 5.- Effect of horizontal-tail incidence on aerodynamic characteristics of model with T-tail and mid M-wing.

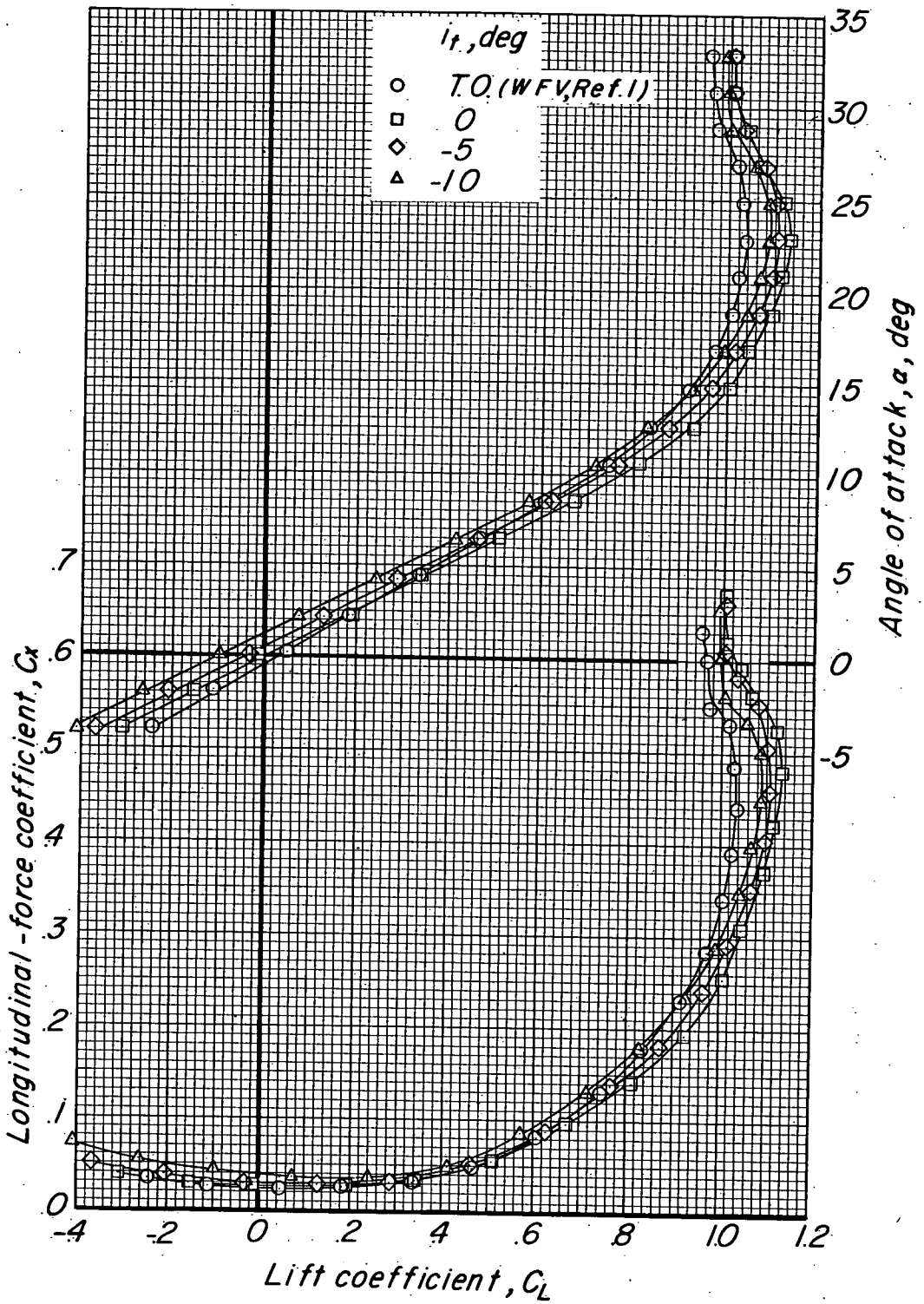

Figure 5.- Concluded.

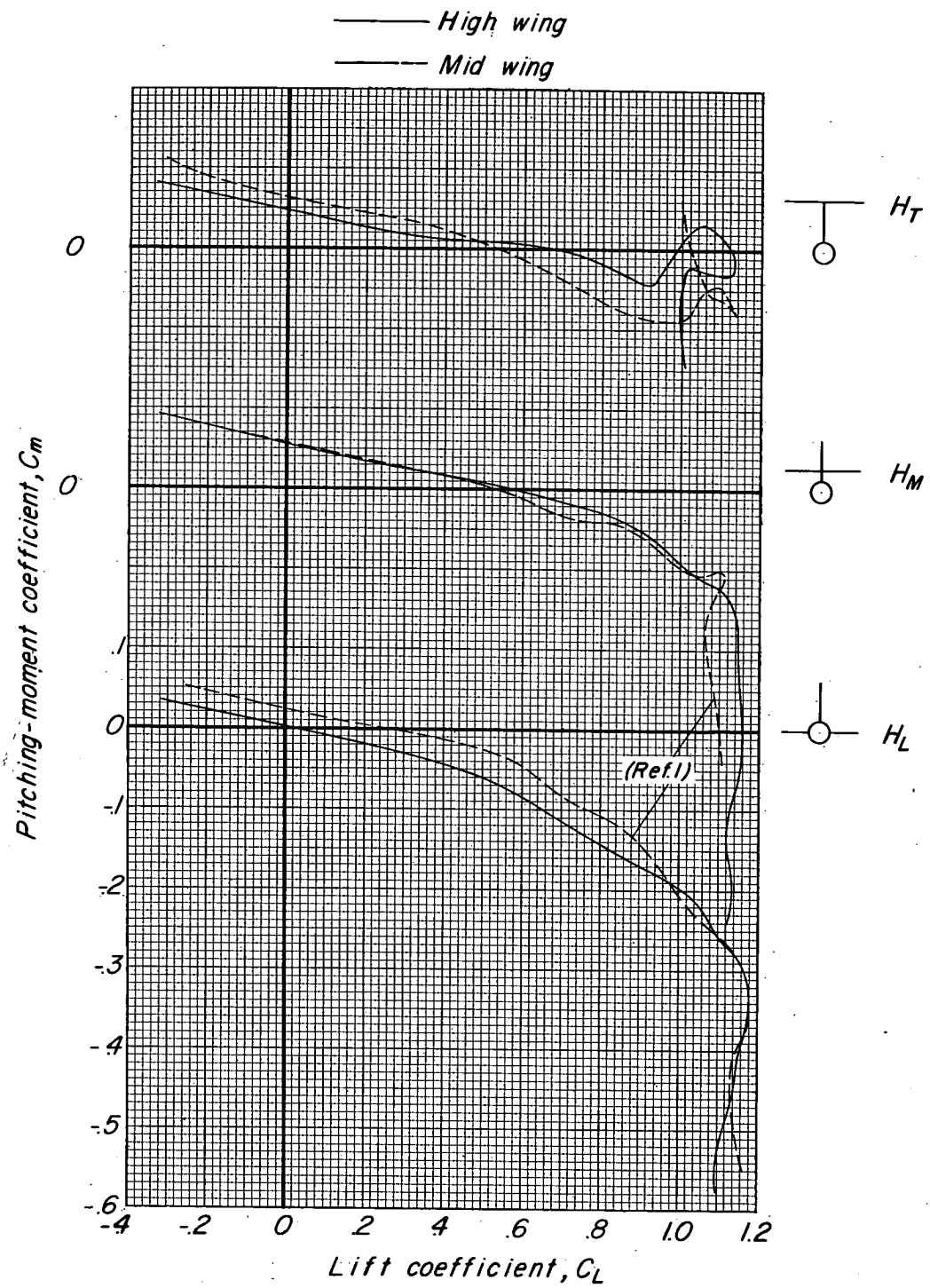

(a) C_m against C_L.

Figure 6.- Effect of wing height on longitudinal stability characteristics of model with M-wing and three horizontal-tail heights. Static margin adjusted to 0.10$\bar{c}$.

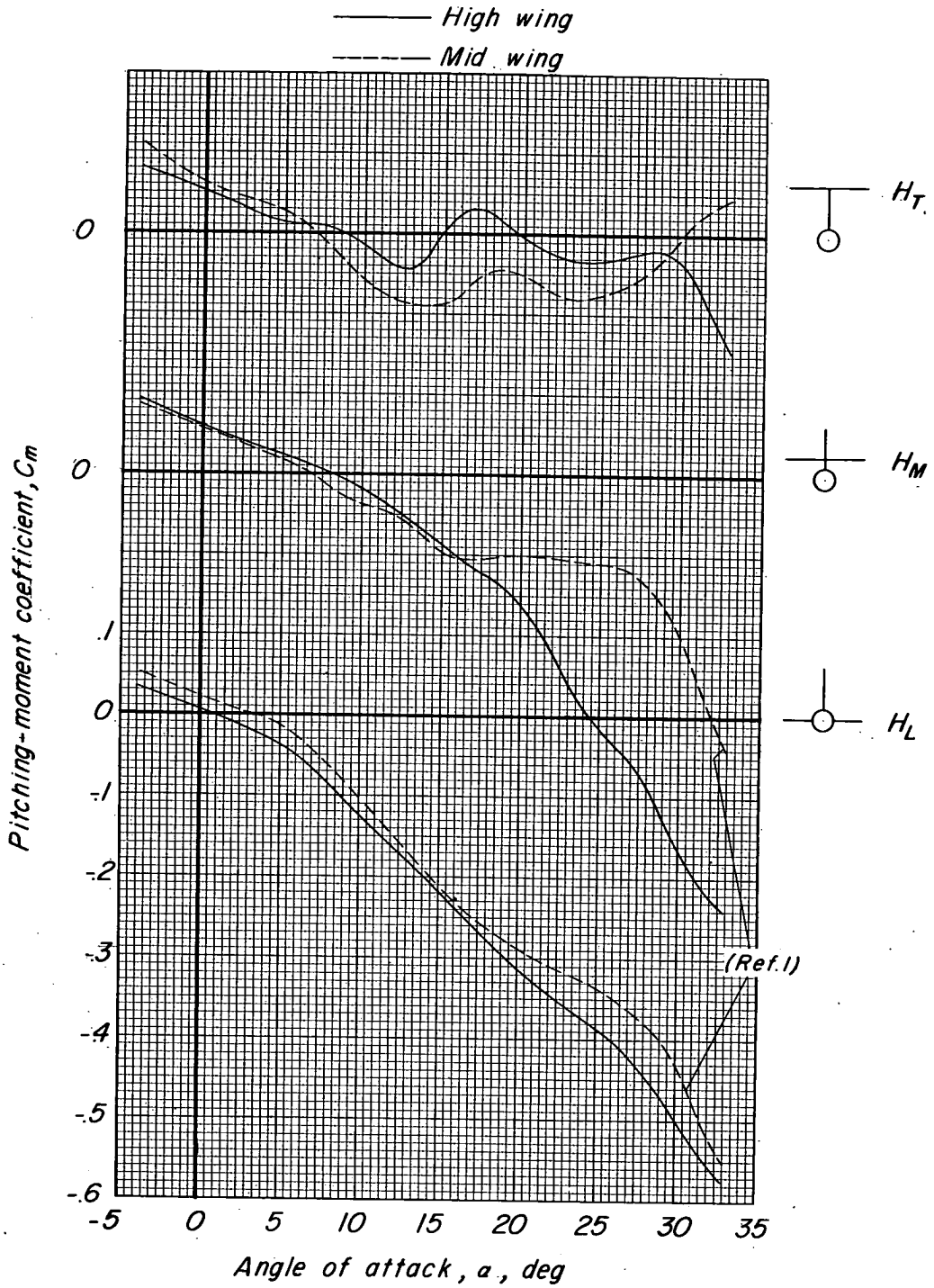

(b) C_m against α.

Figure 6.- Continued.

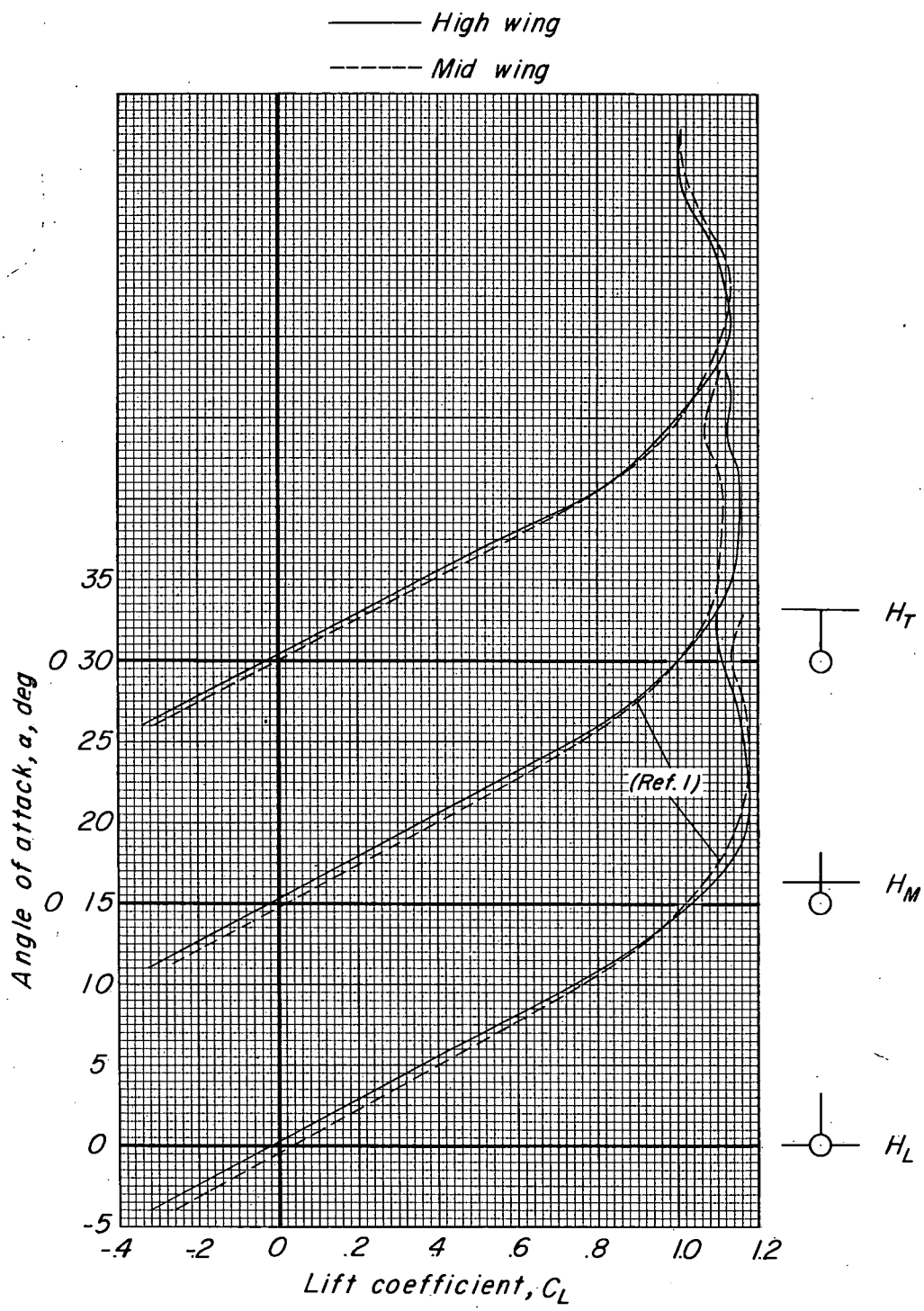

(c) α against C_L.

Figure 6.- Continued.

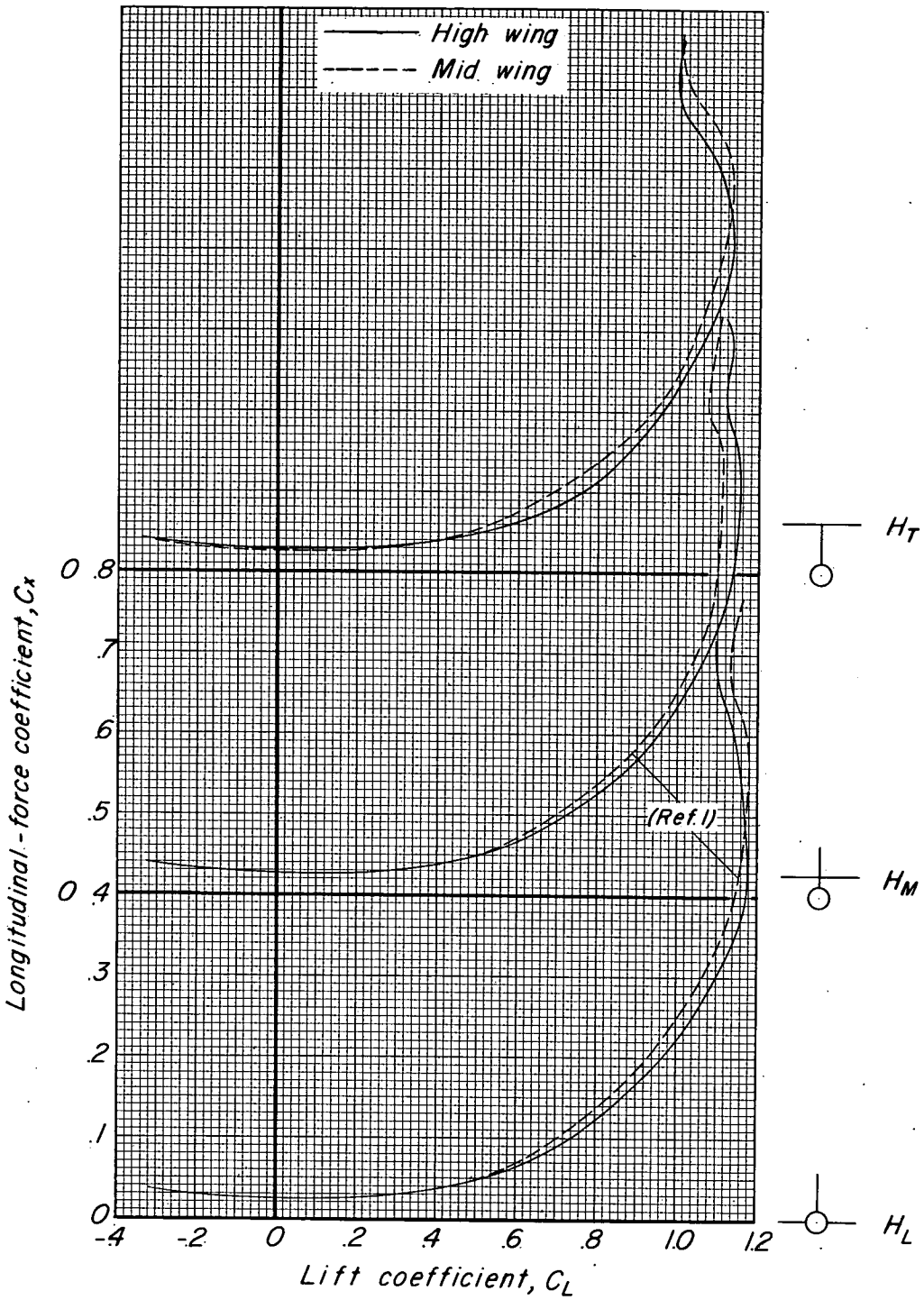

(d) C_X against C_L.

Figure 6.- Concluded.

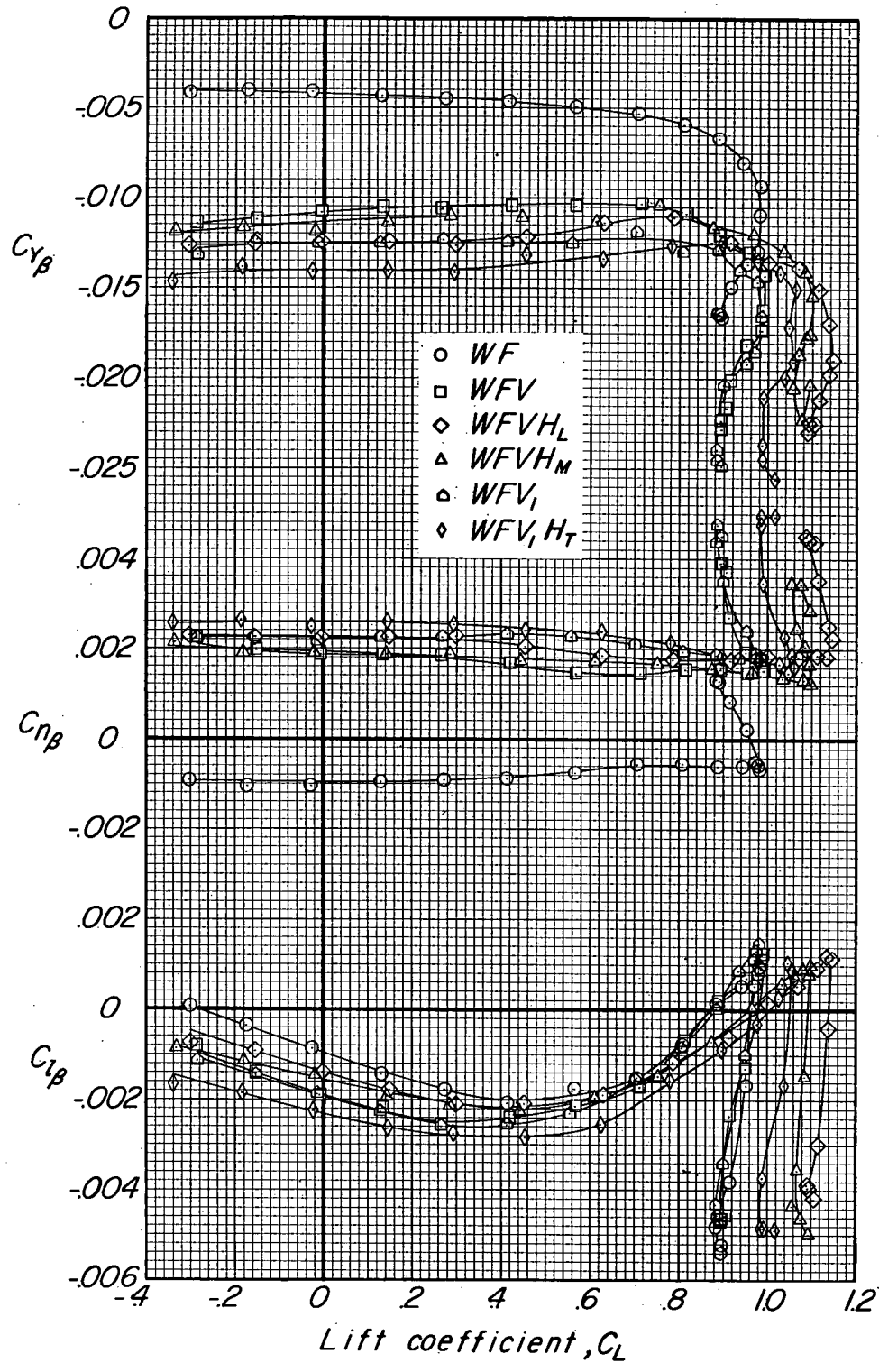

Figure 7.- Effect of the component parts on the lateral stability characteristics of model with high M-wing.

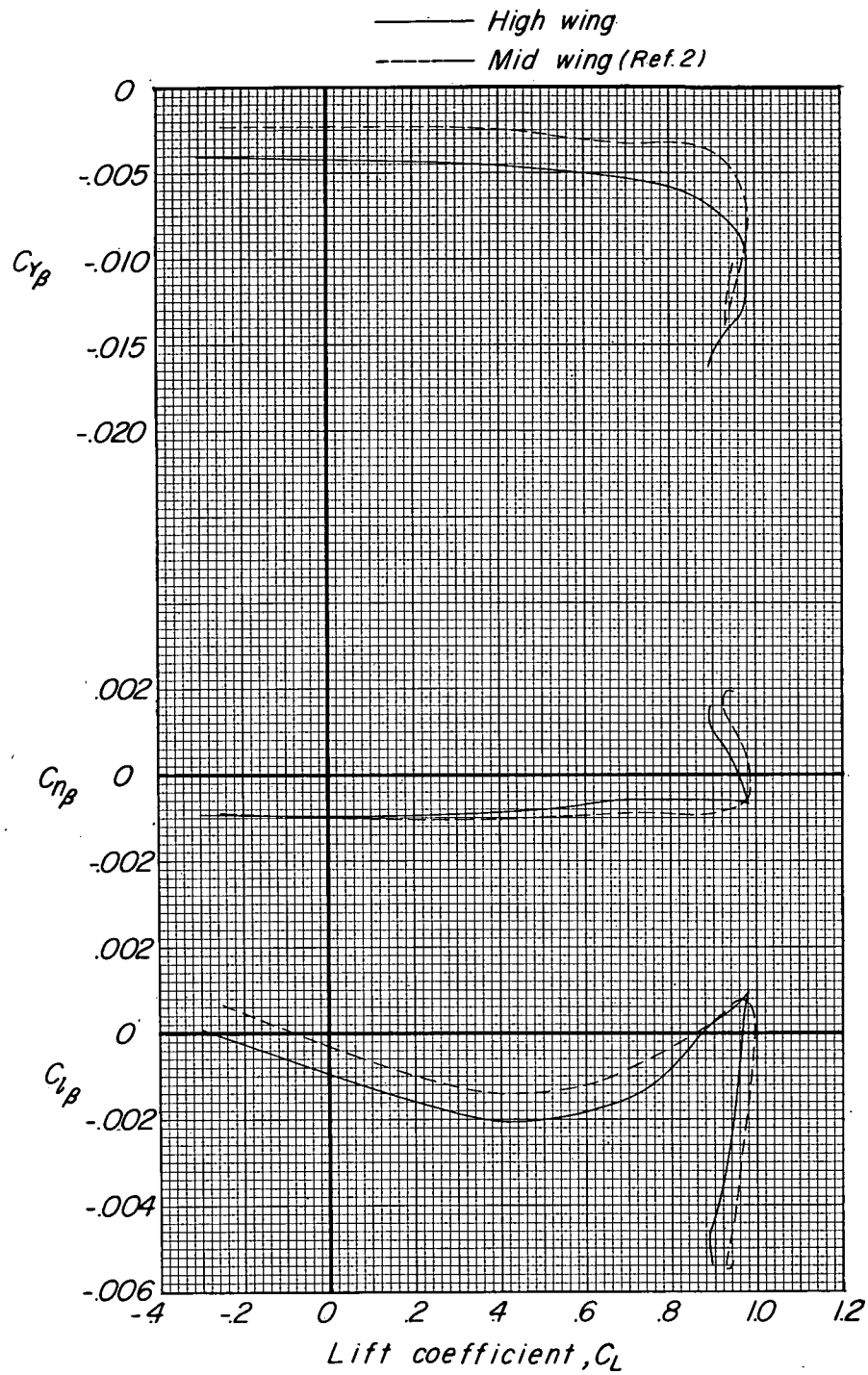

(a) WF.

Figure 8.- Effect of wing height on lateral stability characteristics of model with M-wing.

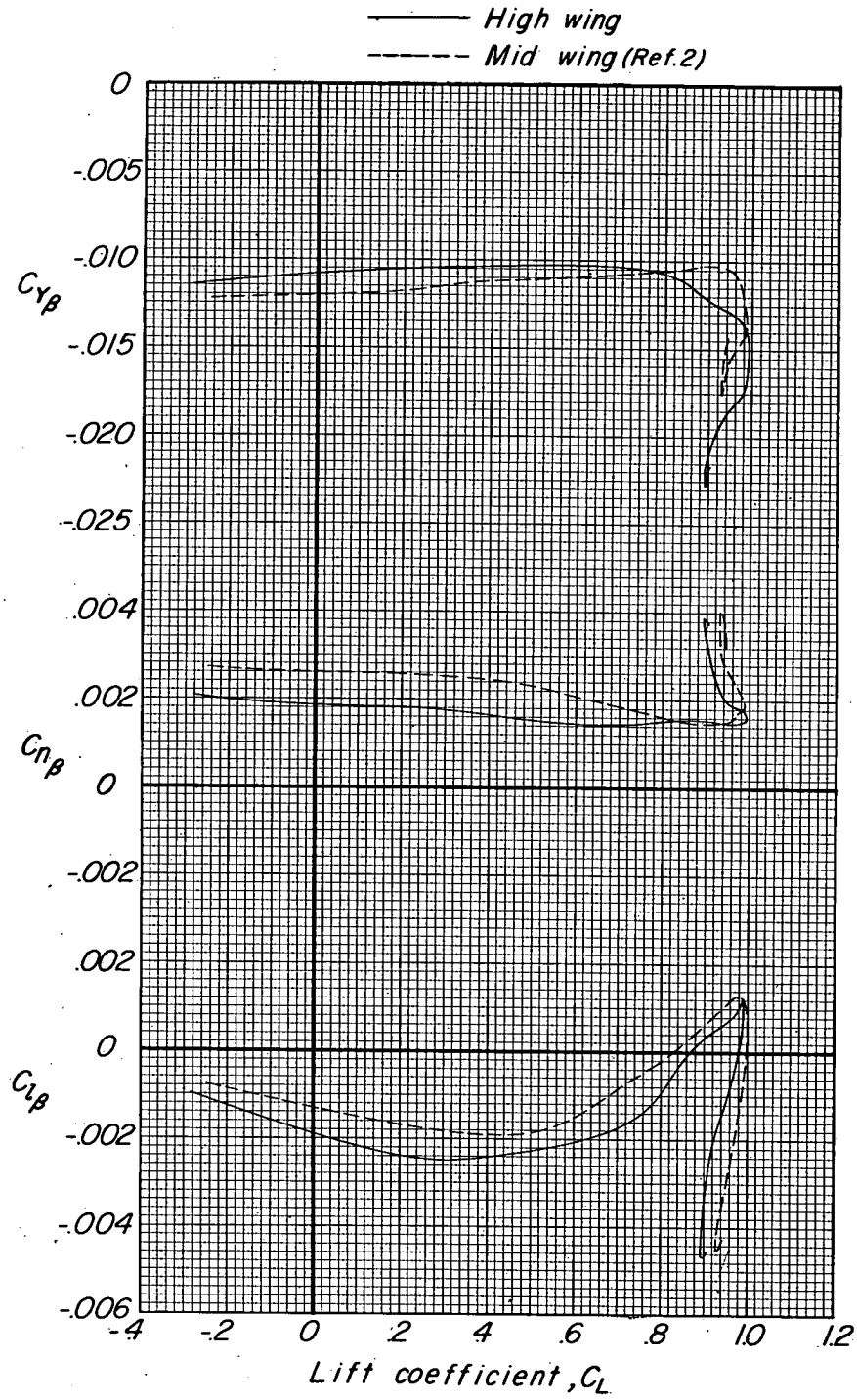

(b) WFV.

Figure 8.- Continued.

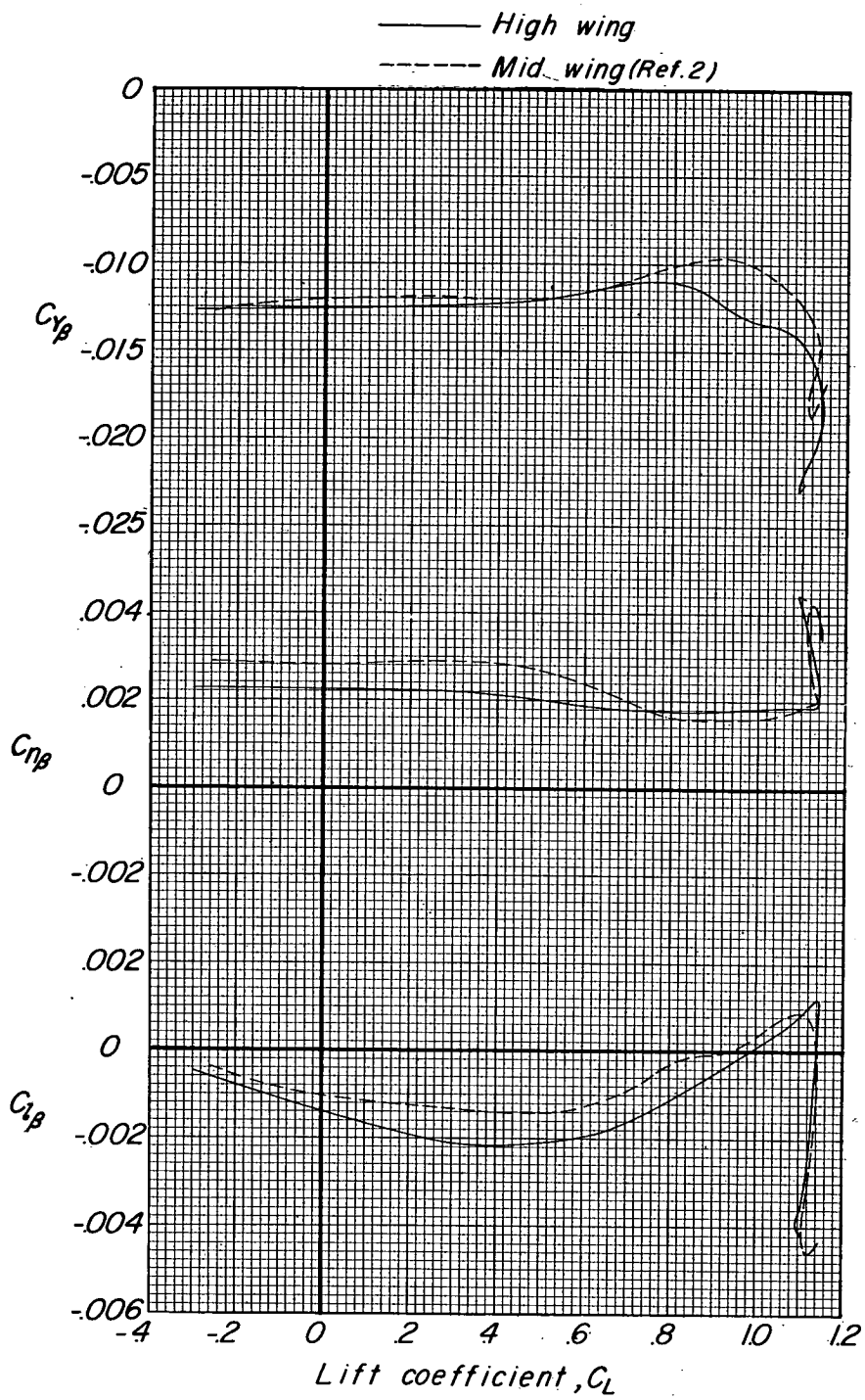

(c) $WFVH_L$.

Figure 8.- Continued.

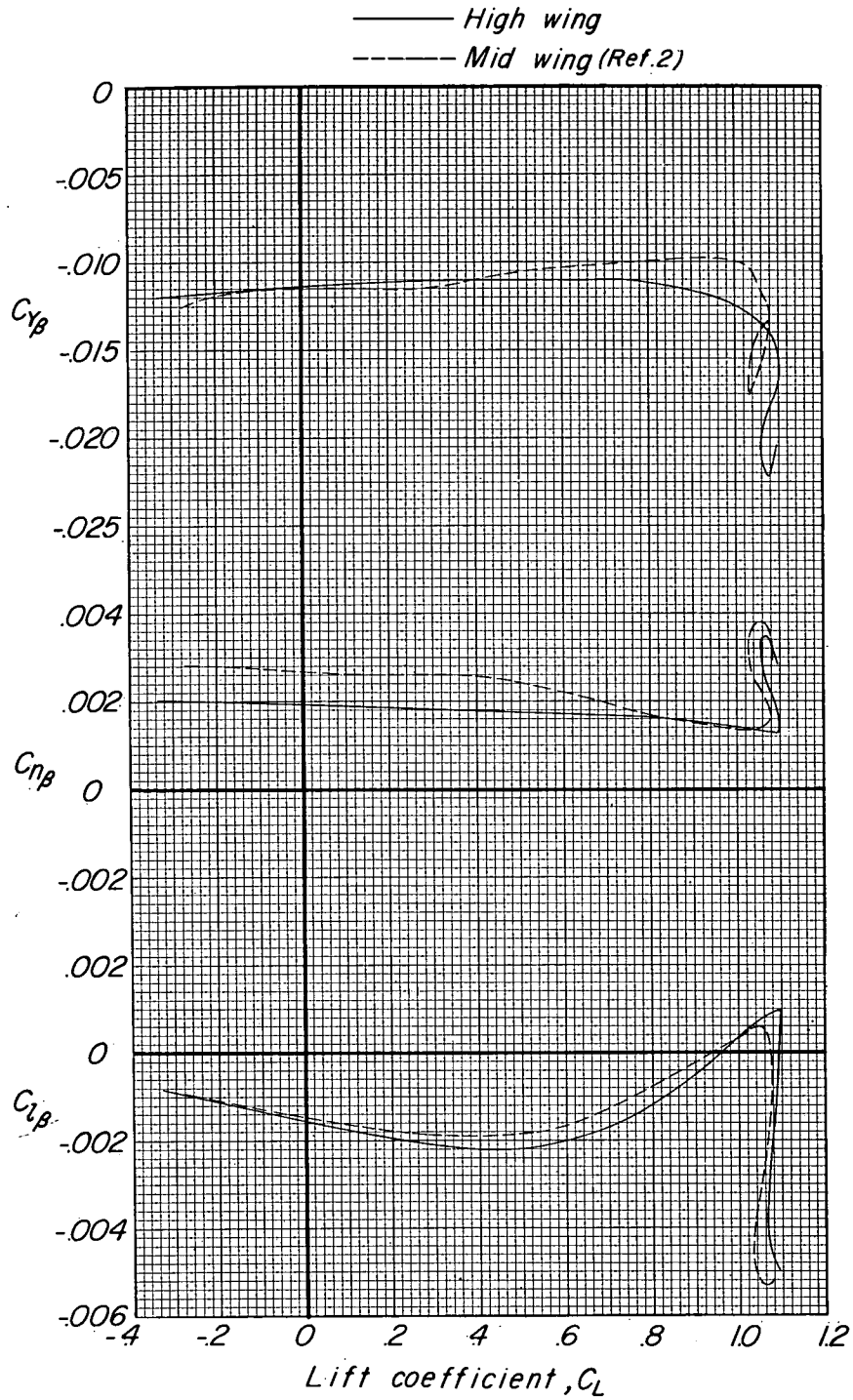

(d) $WFVH_M$.

Figure 8.- Continued.

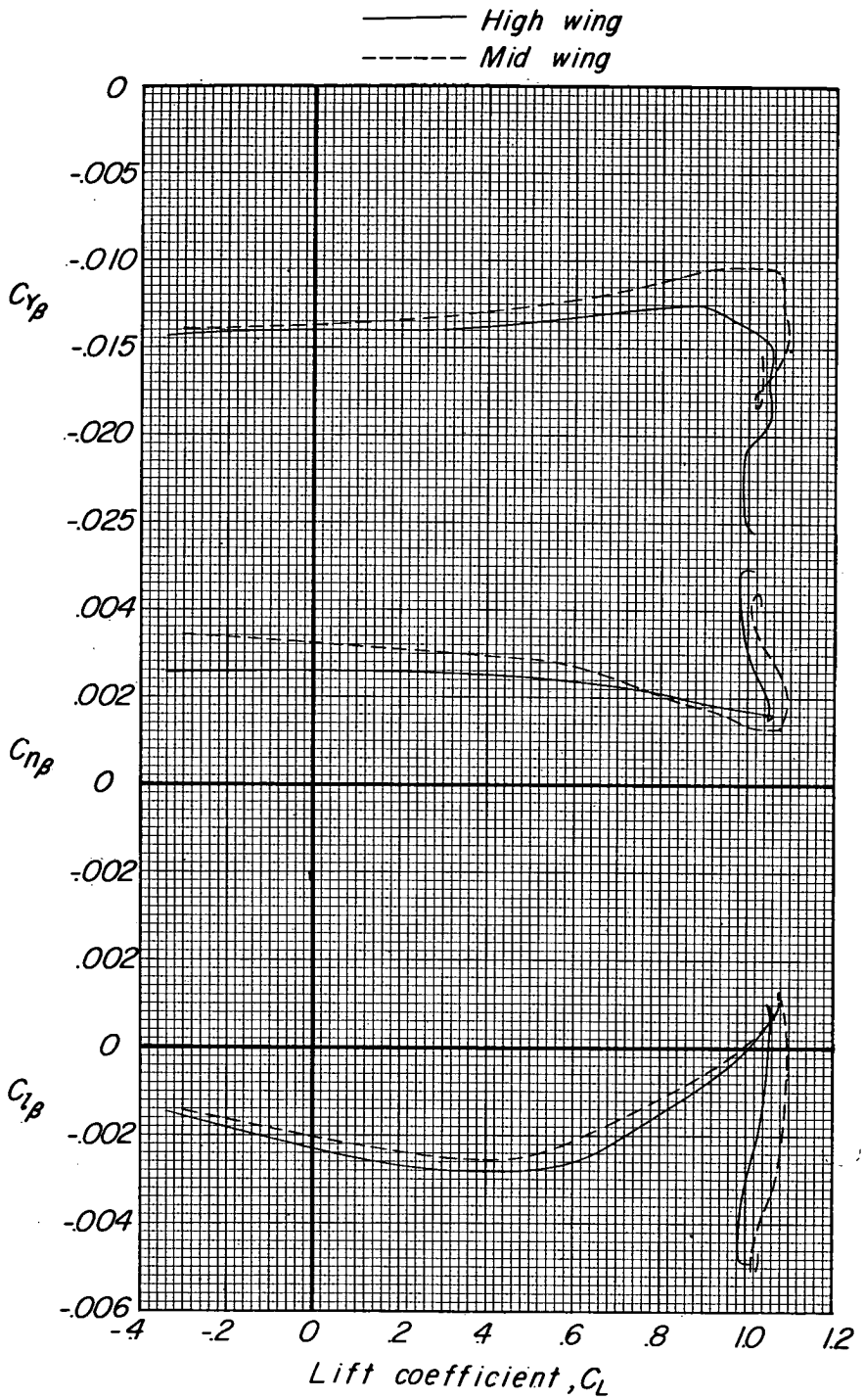

(e) WFV_1H_T.

Figure 8.- Concluded.

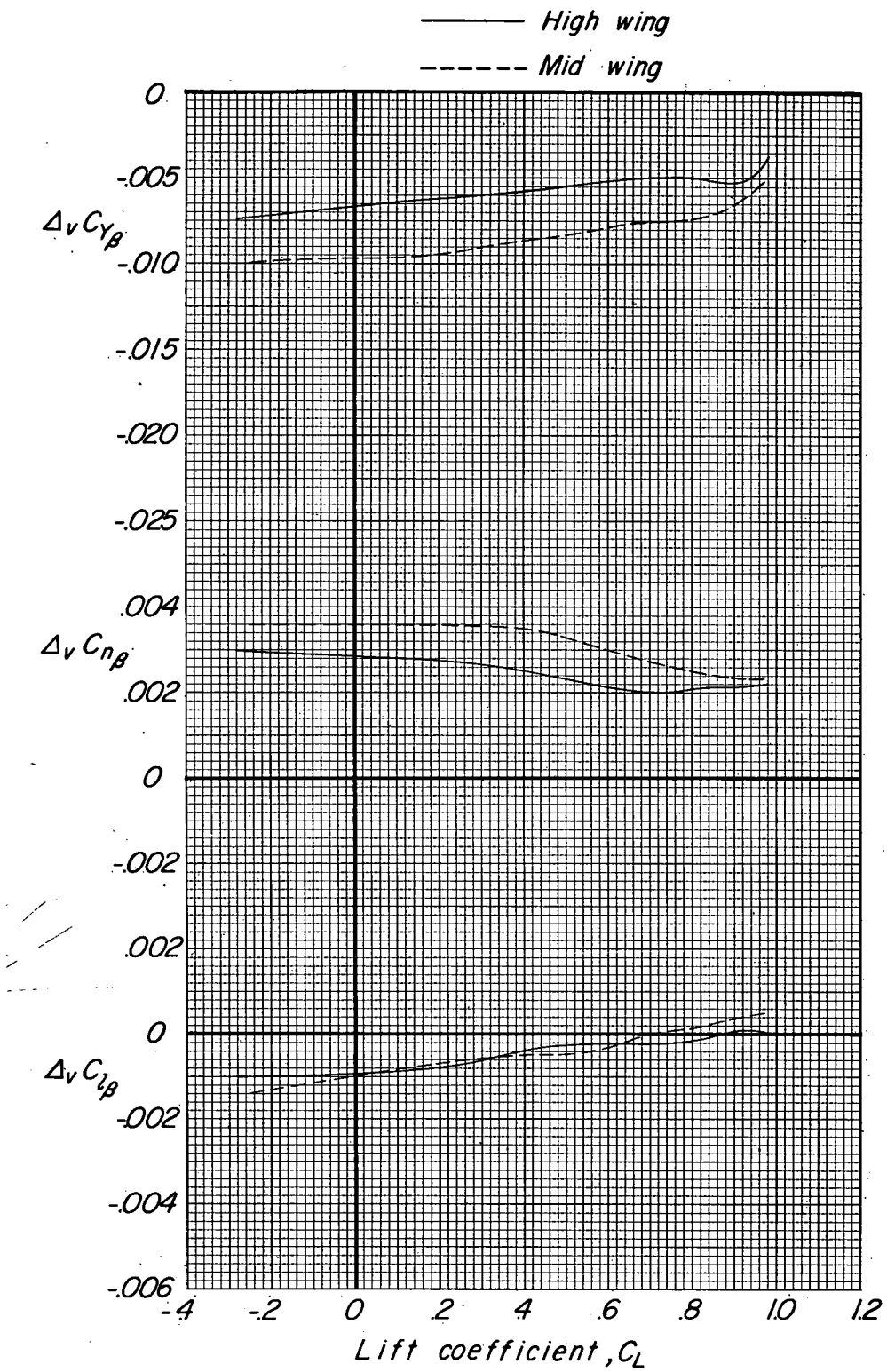

Figure 9.- Effect of wing height on the contribution of the vertical tail to the lateral parameters; horizontal tail off.